Materials and Design 64 (2014) 374–380

Contents lists available at ScienceDirect

Materials and Design

journal homepage: www.elsevier.com/locate/matdes

Hot deformation behavior and microstructural evolution of a modified 310 austenitic steel

Hongying Sun [a,c], Yongduo Sun [b], Ruiqian Zhang [b], Man Wang [a], Rui Tang [b], Zhangjian Zhou [a,*]

[a] School of Materials Science and Engineering, University of Science and Technology Beijing, Xueyuan Road 30, Haidian District, Beijing 100083, China
[b] Science and Technology on Reactor Fuel and Materials Laboratory, Nuclear Power Institute of China, P.O. Box 436, Chengdu, Sichuan 610041, China
[c] School of Mechanical Engineering, Anyang Institute of Technology, West of Huanghe Road, Wenfeng District, Anyang, Henan Province 455002, China

ARTICLE INFO

Article history:
Received 30 June 2014
Accepted 2 August 2014
Available online 12 August 2014

Keywords:
Austenitic stainless steel
Dynamic recrystallization
Precipitates
Electron backscatter diffraction
Grain boundary characteristic distributions

ABSTRACT

To study the hot deformation behavior and microstructural evolution of a new modified 310 austenitic steel, hot compression tests were conducted at the temperature range from 800 to 1100 °C with strain rate of 0.1–10 s^{-1} and strain of 30–70% using Gleeble 3500 thermal–mechanical simulator. The results showed that the serrated flow curves were caused by the competitive interaction between solute atoms and mobile dislocations. There were some coarsened precipitates on the high angle grain boundaries (HAGBs), which facilitated the nucleation of dynamic recrystallization grains. But these precipitates inhibited the growth of the recrystallization grains, and changed the deformation texture in the matrix. Low angle grain boundaries (LAGBs) decreased, while twin GBs and random HAGBs and increased as dynamic recrystallization occurred. Dynamic recrystallization occurred more readily at evaluated temperature or high strain rate. The true stress decreased with the reduction of LAGBs percent. The internal connections between mechanics and microstructures were also discussed.

1. Introduction

Austenitic stainless steels are important candidate materials for advanced nuclear power industry due to their high creep strength and excellent corrosion/oxidation resistance [1]. Therefore, austenitic stainless steels have been investigated in many extended ways, including their deformation behaviors. Hot deformation is an important approach for steels, because it involves a complex microstructural change, which may optimize the mechanical properties of the finished product [2]. To avoid the defects produced during deformation, it is necessary to investigate the microstructural evolution during hot deformation process under various conditions, as reported by Tan et al. [3] and Belyakov et al. [4]. Over the last decade, a lot of research works have been carried out on hot deformation behavior of austenitic stainless steel, mainly were AISI 304 [5], 304H [6] and AISI 316L steel [7]. Dehghan-Manshadi et al. [8–10] have performed a series of studies on the dynamic recrystallizations (DRX) of 304 austenitic stainless steel. According to their studies and some other research works of a Cr–Ni–Mo–Cu–Ti–V steel [11] and a 15Cr–15Ni–2.2Mo–Ti modified austenitic stainless steel [12], the microstructural evolution in the hot deformed steels can be described as: the original grain boundaries (GBs) elongate along the deforming direction and GB serrates or bulging generates and some new DRX grains nucleate at the serrated GBs. The DRX grains nucleate at HAGBs of original grains, and then the new DRX grains coarsen, until these DRX grains become connected with each other and cover the boundaries gradually, which is called "necklace" structure [13]. Thus, the first "necklace" structure is shaped. Similarly, the second and third layers of "necklace" structures formed, till the full DRX is achieved.

Many investigations have clearly shown that the occurrence of DRX depend greatly on composition [14], initial grain size [15] and precipitates [16] of the materials characteristics and processing parameters [17]. Therefore, to obtain fine or ultra-fine grain structural materials, most of researchers have focused on the effects of processing parameters and original grain size on the microstructural evolution [18]. Wahabi et al. [19] studied the effect of initial grain size on DRX behavior of AISI 304 stainless steel, and found that the occurrence of DRX was mainly contributed by fine grains. Actually, the influence of processing parameters on the DRX is complicated. For the vast majority of austenitic stainless steels, especially those contain strong carbide-forming elements such as Cr and Mo, the precipitates may actually play critical roles in the forming process. For example, Momeni et al. [20] found that the dynamic precipitation took place in the super-austenitic stainless steel type 1.4563 during hot deformation. They called this precipitation as "Strain Induced Precipitation" (SIP). The strain stored

* Corresponding author. Tel./fax: +86 10 62334951.
E-mail address: zhouzhj@mater.ustb.edu.cn (Z. Zhou).

http://dx.doi.org/10.1016/j.matdes.2014.08.001
0261-3069/

Table 1
Chemical composition of the modified 310 austenitic stainless steel (wt.%).

Ni	Cr	Si	Ti	Zr	V	Mo	Mn	C	Cu	Fe
20.22	19.56	0.65	0.20	0.2	0.15	2.15	0.13	0.10	0.12	Bal.

energy was consumed by SIP, and SIP was a main competitor for DRX during hot deformation. Therefore, the SIP inhibits the process of DRX, and increases the recrystallization temperature.

In addition, another case should be considered is the second phases formed during solidification, such as preferential inclusions and first precipitates. These hard and brittle precipitates result in stress concentration and lead to high store energy in local region [21]. The influence of them on the DRX may be different. However, the influence of these precipitates on the deformation behavior and dynamic recrystallization was only investigated in a limited way. Therefore, it is significant to investigate the influences of these coarsened precipitates on the DRX during hot deformation.

In this study, the effect of hot deformation parameters (temperature, strain rate and strain) on the microstructural evolution of a modified 310 austenitic stainless steel was investigated. The new steel was developed in the laboratory for advanced nuclear power industry. In addition, the influences of the precipitation and some precipitates on the DRX, grain boundary character distributions (GBCDs) and texture were also discussed based on the electron backscatter diffraction (EBSD) analysis.

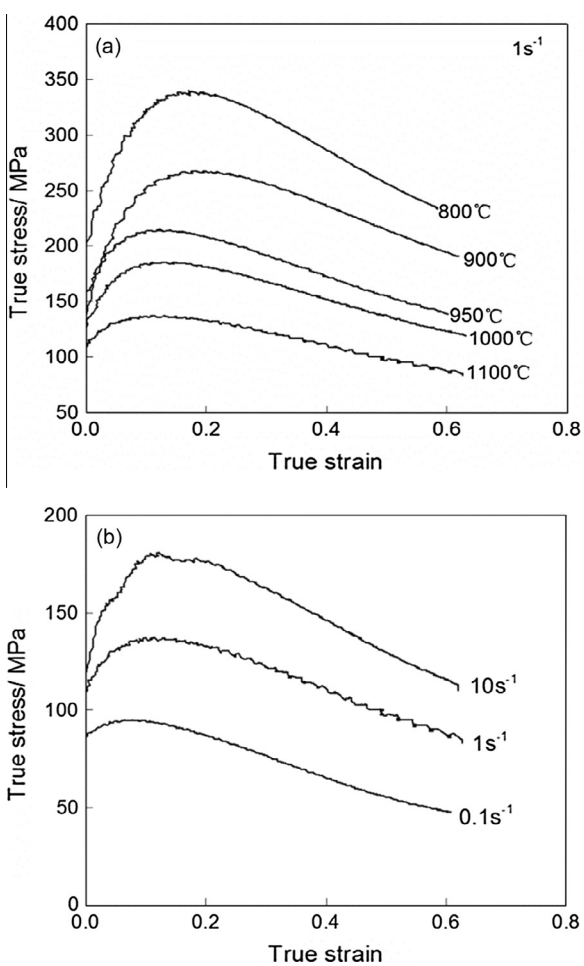

Fig. 1. Flow curves of super-austenitic stainless steel under different deformation conditions (a) 1 s^{-1}; (b) T = 1100 °C.

2. Material and methods

2.1. Material preparation

The chemical composition of the modified 310 austenitic steel is shown in Table 1. The specimens of thermo-mechanical simulation compression were machined from the forged modified 310 austenitic stainless steel. They were cylindrical samples with 8 mm in diameter and 15 mm in height (Φ 8 × 15 mm). In order to reveal the microstructure, specimens were cut along the longitudinal axis. Then, they were grinded to 1500 grade by using sand paper and electrochemical etched in a solution of $HClO_4$:CH_3COOH = 5:95 (volume fraction) at 40 V and 0 °C for 20–40 s.

2.2. Hot deformations

The thermo-mechanical simulation compression test was carried out on a Gleeble-3500 thermal–mechanical simulator at constant compression strain rate and invariable temperature. The specimen was heated to 1200 °C with the heating rate of 10 °C s^{-1} and held for 10 min, then cooled to individual deformation temperatures with the cooling rate of 5 °C s^{-1} and held for 5 min. Almost all compression ratios were 50% (ε = 0.68) at 0.1 s^{-1}, 1 s^{-1} and 10 s^{-1} strain rates. And the temperature is from 800 °C to 1100 °C. Two additional specimens were compressed to 30% (ε = 0.34), 70% (ε = 1.2) respectively at 1100 °C and 1 s^{-1}. After compression, the specimens were quenched into water directly.

2.3. EBSD experiments

Microstructures of all deformed samples were examined with EBSD, and some were investigated by optical microscope (ZEISS Observer.A1 m) and Scanning Electron Microscope (SEM, FEI-200)

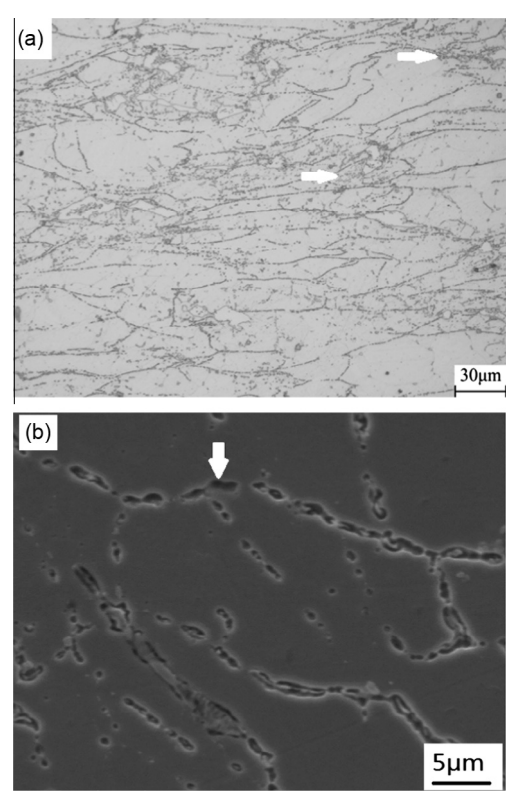

Fig. 2. Complex precipitates observed at grain boundaries (a) 900 °C, 1 s^{-1}, 50% and (b) 1100 °C, 1 s^{-1}, 50%.

with an Energy Dispersive Spectroscope (EDS). And the step size changed from 1.2 μm to 3 μm with distinct hot working conditions. The investigated area was about 0.2 mm^2 in each specimen. Data analyses were performed using Chanel 5 HKL Project Manager software in order to collect microstructure and determine measurements from all specimens. The Palumbo–Aust criterion ($\Delta\theta = 15°\Sigma^{-5/6}$) [22] was used to analysis and categorize GBs by their misorientation descriptions automatically. GBs were divided into three groups: random HAGBs (misorientations greater than 15°, shown as black lines), twin boundaries (misorientation of 60° about a 111 axis with angular tolerance of 0.5°, shown as green lines), and low misorientations (blue and red lines), which are some substructures, including sub-grain boundaries, dislocation walls or in a general way with dislocation density.

3. Results and discussion

3.1. Stress–strain curves

As shown in Fig. 1, the flow stress rapidly increased with the increase of strain till the stress reached the maximum (peak stress) value. Subsequently, the stress dropped continuously with increasing strain. The dynamic recovery process of tested steel is a long term, so it is difficult to reach the steady-state stress under the strain ($\varepsilon = 0.68$).

The curves of different strain rates showed different apparent characteristics (Fig. 1(b)). The flow curve that deformed at the highest strain rate (10 s^{-1}) exhibited a feature of serrations, which showed larger fluctuations and waves at high stress. As the strain rate decreased, serrations fade away till disappeared at the strain rate of 0.1 s^{-1}. The fluctuation extents of the flow stress increased with temperature. Furthermore, the flow curve of specimen hot deformed at the highest strain rate is characterized by a short plateau following the peak stress, and a prolonged work hardening region with slight increase in the stress. The following section is a small flat roof. This trend is related to the interior structure of samples which some complex Cr, Mo carbides were formed. The existence of strong carbide formers, Cr and Mo, in the studied alloyed steel corroborated the formation of complex carbides. The precipitation may be stimulated by the influence of imposed strain. Fig. 2 shows the microstructures containing precipitates (signed by white arrows). The EDS result showed the precipitates at GBs were complex carbides of Cr, Mo, Ni and Fe, having the composition of 3.24C–6.06Mo–55.5Cr–28.06Fe–7.14Ni (wt.%).

The serrated feature of flow curves can be attributed to a competition between DRX and SIP. At low temperatures, the formation of carbides resulted in the pinning effect on the grain boundaries.

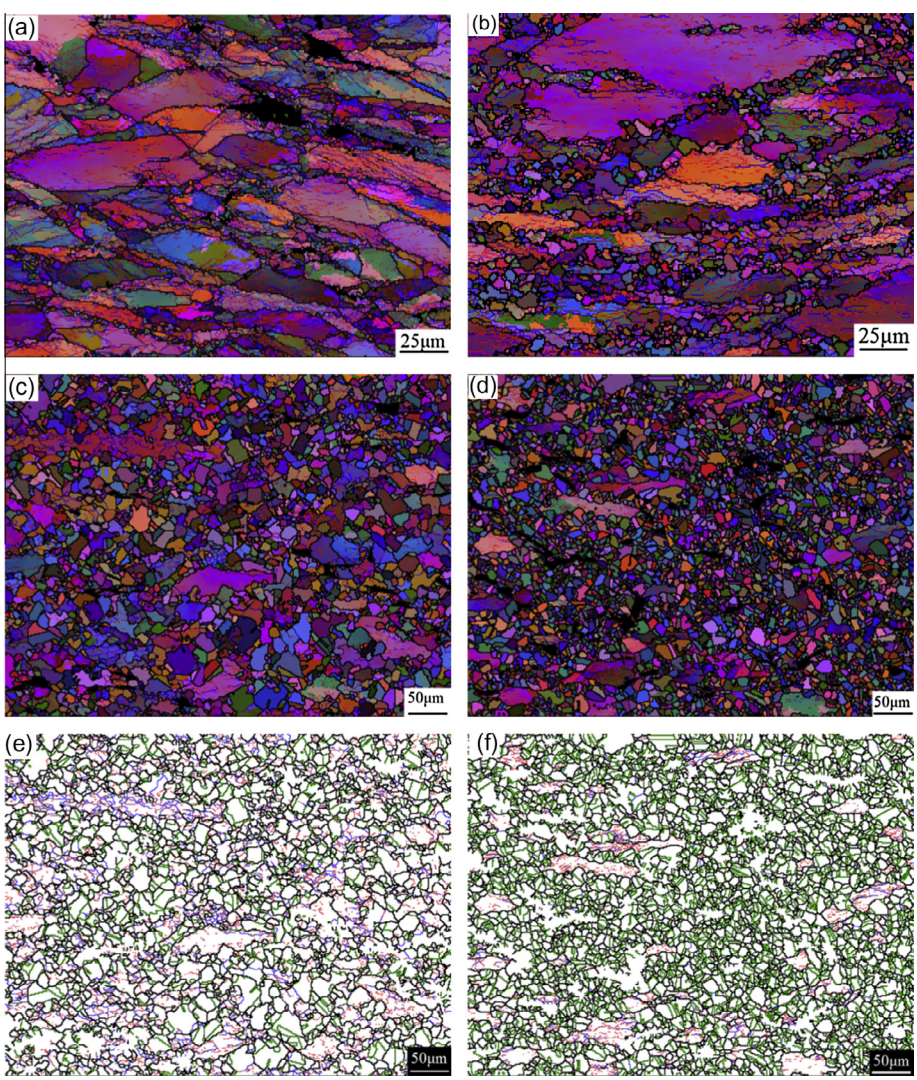

Fig. 3. Microstructure of specimens at different deformation conditions and corresponding grain boundary maps (a) 900 °C, 0.1 s^{-1}; (b) 1000 °C, 0.1 s^{-1}; (c) 1100 °C, 0.1 s^{-1}; (d) 1100 °C, 10 s^{-1}; (e) grain boundary map of (c); (f) grain boundary map of (d).

This effect in turn retarded the DRX by preventing the movement of dislocations and the local bulging of GBs. In this manner, an increment of flow stress in stress–strain curve was required to overcome the pinning or release the bulges from precipitates, whereas the following decline might be a result of the stress relaxation caused by the free movement of dislocations or the growth of bulges after relieving from the pinning of precipitates. This process is repeated, resulting in a several oscillations of stress–strain curves. Both the precipitation and GB mobility are diffusion-controlled processes [20]. Thus, the higher the temperature, the greater the interaction between precipitation and DRX will be. At the highest strain rate, i.e., 10 s^{-1}, the stored energy was higher, and the time for the occurrence of SIP was short, so the driving force for DRX still remained higher. Therefore, the DRX was dominated, but SIP was not completely restricted. The shorter time for coarsening of the new precipitates resulted in fine particles which had a significant pining force to the GBs [23]. Therefore, the flow stress followed its unnatural shape.

3.2. Microstructural evolutions

Microstructures and the corresponding GB maps of different deformed specimens are shown in Fig. 3. Fig. 3(a) denotes the deformation of the tested steel at lower temperature. Some grains are elongated along the deformation direction and become pancaked grains. On the GBs, a large number of HAGBs become serrated or bulged, and some finer DRX grains are observed. This result is accordance with previous work. When DRX is activated on GBs, the bulge mechanism is assumed to operate [9]. Thus, a number of these new smaller DRX grains are formed mainly through dynamic bulging mechanism. Additionally, there are some precipitates (black areas) at triple junctions, and more new small grains are evolved around coarsened precipitates (Fig. 3(a)), forming the first layer of "necklace" structure. However, there are still small quantities of GBs which shows no sign of DRX. This result indicates that the inhomogeneous microstructure primly provides a large strain gradient and a high local dislocation density. This inhomogeneous microstructure in the DRX process is very important and favorable to DRX nucleation [9].

More GBs become serrated and bulged, as the temperature grows. Then the first layer of "necklace" structure decorates most of the GBs, even at areas without precipitates. At the same time, some GBs are covered by the second or third layer "necklace" structures, as shown in Fig. 3(b). It is important to note that the grain size of new DRX in Fig. 3(b) is larger than that in Fig. 3(a). With a rise of temperature, new grains generated continuously (Fig. 3(c)). At both high temperature and high strain rate, an almost full DRX microstructure is found as shown in Fig. 3(d). Still several pancaked grains far from the precipitates are observed in Fig. 3(d). Compared with Fig. 3(d), DRX in Fig. 3(c) occurs more favorably in the specimen deformed at high strain rate because of high dislocations that promotes the nucleation of new DRX grains [8].

In Fig. 3(e) and (f), random HAGBs are indicated by black line, twining GB by green line, LAGB in red, and subgrain boundaries in blue. The fraction of twining GBs obviously increases with the amount of DRX grains. Moreover, most of twining GBs located in the DRX grains have no dislocation. On the contrary, the LAGBs and sub-grain boundaries are in pancaked grains. This result confirms that the distributions of various GBs are different.

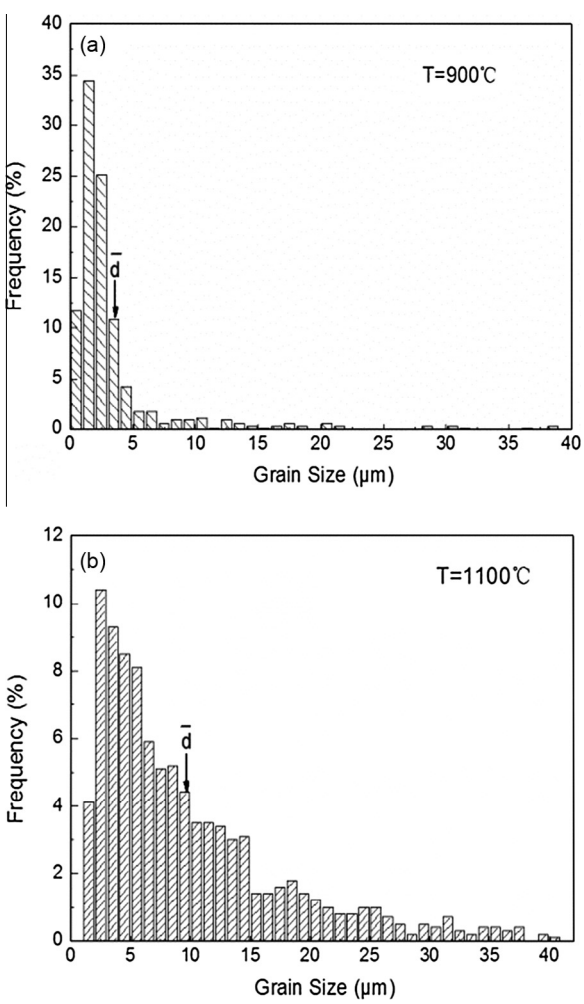

Fig. 4. DXR grain size distribution at 0.1 s^{-1} and deformed to 0.68 (a) $T = 900$ °C; (b) $T = 1100$ °C.

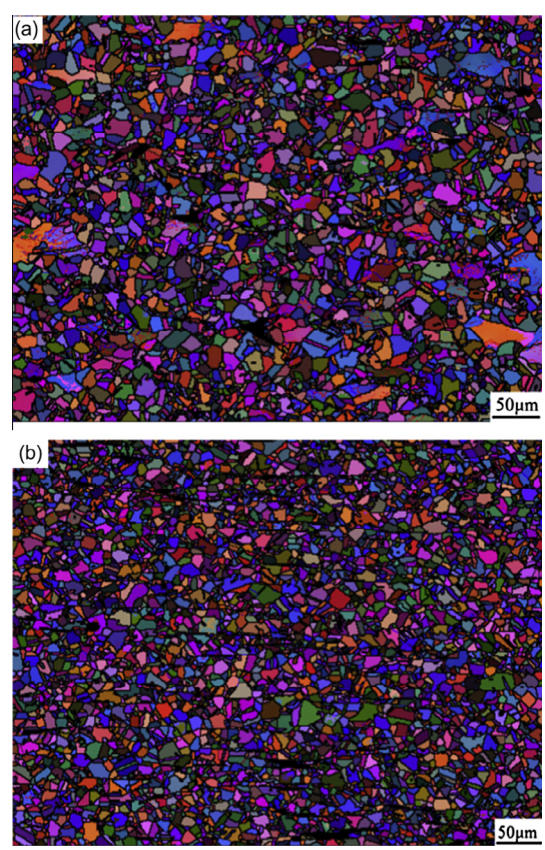

Fig. 5. Microstructures of specimens at 1100 °C and 1 s^{-1} strain rate to different strains (a) $\varepsilon = 0.34$; (b) $\varepsilon = 1.2$.

As shown in Figs. 3 and 4, the recrystallized grain size is significantly affected by deformation parameters. When the sample was deformed at 900 °C and 1 s^{-1}, most of the recrystallization grain sizes are rather small, less than 5 μm. In the sample deformed at 1100 °C and 1 s^{-1}, the percentage of small grains is greatly reduced, while the number of grains with larger size obviously increases. At a certain strain and strain rate, the recrystallized grain size distribution becomes dispersed and increases with temperature. When the deforming temperature rises from 900 °C to 1100 °C, the average recrystallization grain size grows from 3 μm to 9 μm (see Fig. 4(a) and (b)). This result shows that the DRX grain which formed at the higher temperature is actually coarser than those formed at lower temperature.

With the increase of strain and further deformation, new grains proceed to form and show no significant change in the DRX grain size (see Fig. 5). The size of grain surrounding the second particles was not lager than other grain size, though they were early formed. The coarsened precipitates were believed to inhibit the growth of the recrystallize grains. However, it is obvious that the microstructure in larger strain specimen is more homogeneous than in the smaller one, which is a mixed structure of DRX grains and a few pancaked grains. This is because that the extent of DRX in the samples is different, and nearly a completed DRX microstructure has been involved in the sample exhibited in Fig. 5(b). It can be inferred that the strain has effect on the occurrence of DRX but no visible influence on the DRX grain size [1,8,9].

In Figs. 3 and 5, the nucleation mechanism of new DRX grains can be obtained through microstructures observation. As shown in the figures, the early stage of DRX, as well as the grains growth process is involved in the influence of second particles. These second particles are favorable nucleation sites for DRX, due to the presence of high local dislocation densities, which attribute to strain incompatibility between the precipitates and the matrix. It can be deducted from Figs. 3 and 5 that these coarsened precipitates provide the nucleation positions for recrystallization grains, but also inhibits the growth of the recrystallize grains.

3.3. Misorientation evolutions

Previous studies have been carried out to investigate the effect of GBCDs on material properties. The results showed that high fraction of twin GBs were beneficial for comprehensive properties of materials, such as remarkable inter-granular corrosion resistance and ductility properties [24]. So it is necessary to study the evolutions of GBCDs during deformation. As shown in Fig. 6, specimen at low deformation temperature contains more LAGBs which are formed by dislocation cumulating during the deformation. Several low misorientation (~1°) boundaries are formed in the specimens deformed at 900 °C and 1000 °C, and most of the misorientation angles are less than 15°. Nevertheless, it is clear that there are more fractions of 2° boundaries and twin boundaries (about 60°) in Fig. 6(b). With the rise of temperature, low misorientation (~1°) disappeared and the 2°GBs are nearly the same of that in Fig. 6(b). In addition, the misorientations between 15° and 60° evidently increase, especially the twin boundaries. In this condition, dynamic recovery processes fade away, and the dynamic recrystallizations lie in a dominant status, and the corresponding microstructure is shown in Fig. 3(c). It is found that sub-grain boundaries (~2°) are dominantly affected by deforming temperature, and LAGBs slowly decreased, while HAGBs

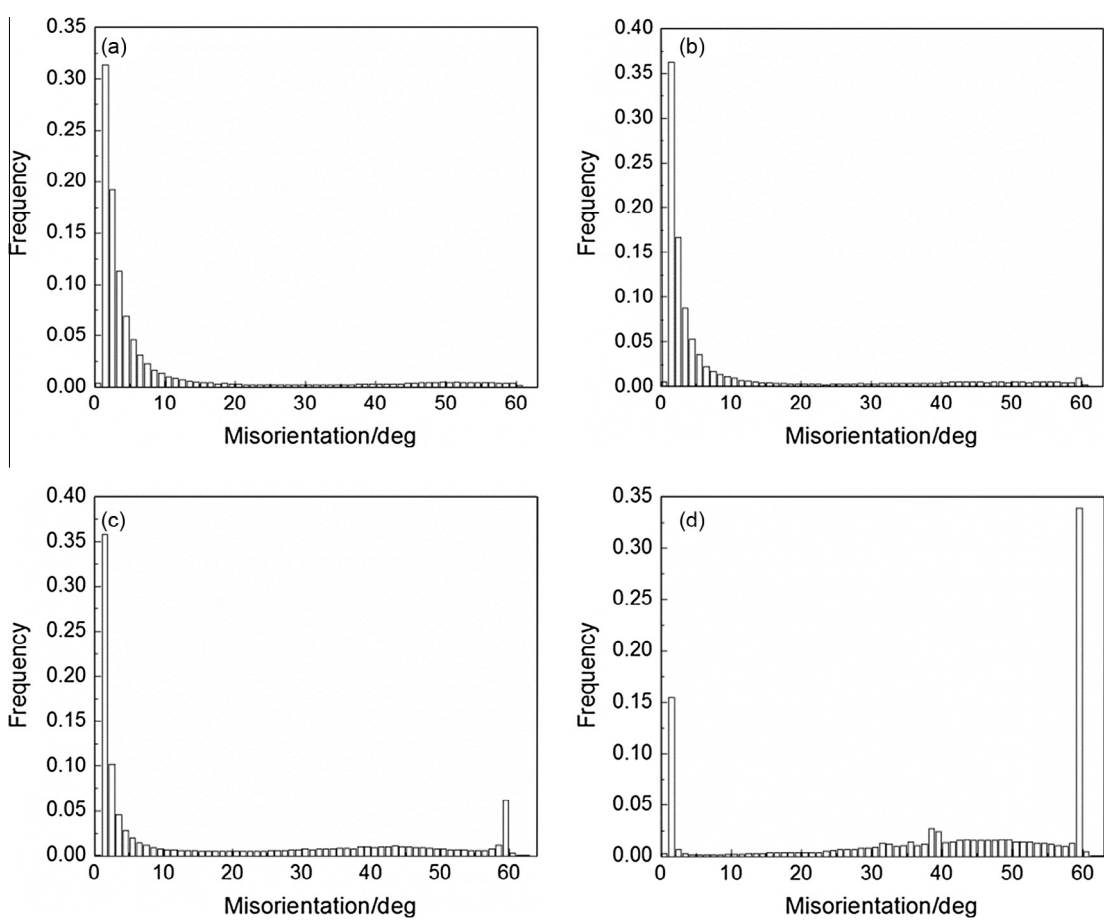

Fig. 6. Grain boundary characteristic distributions at different deformation conditions (a) 900 °C, 0.1 s^{-1}, 50%; (b) 1000 °C, 0.1 s^{-1}, 50%; (c) 1100 °C, 0.1 s^{-1}, 50%; (d) 1100 °C, 1 s^{-1}, 50%.

gradually increased with the increase of temperature, and finally result in the occurrence of DRX.

From Fig. 6(c) and (d), the large differences in many types of GBs fractions, such as the random HAGBs, twin GBs and LAGB, can be found. In Fig. 6(d), the average GB misorientation is around 45°, and twin GBs abruptly increase. However, LAGB evidently decrease. The major reason of this change was supported by the analysis of Section 3.2, in which the high strain rate caused strain store energy raising and promoted the occurrence of the DRX. The presence of the twin GBs in the microstructure demonstrated that formation of recrystallization twins was an important phenomenon during DRX of this tested steel.

3.4. Effect of second phase on texture

In addition to the austenitic microstructure, many coarsened second particles are observed in Figs. 3 and 5. They break-up matrix uniform and shape some turbulences, such as the inhomogeneous precipitates-containing microstructure in the sample of Fig. 3(a). Except for the second particles, the microstructures can be classified into two types: one is the finer DRX grains surrounding the particles, the other is elongated pancaked grains, which are far from these particles (Fig. 7(a)). The textures in different structural areas are shown in Fig. 7(b) and (c) respectively. It is noticeable that the distinct deformation texture is developed in the single-phase austenitic at pancaked grain area marked as "A". The texture of the area in the black rectangular which contains many coarsened particles is veritably weakened (peaks less than 3 as show in Fig. 7(c)). This result may involve that the large second-phase particles randomize the deformed texture in the adjacent area [25,26]. Another reason which is deduced is that the second phases are surrounded by many DRX grains, which are equiaxial and without dislocation or texture. Therefore, it is unreasonable that the deformation textures of particles-containing materials are investigated with the entire regions because some important information on the internal details of local area may be lost or changed.

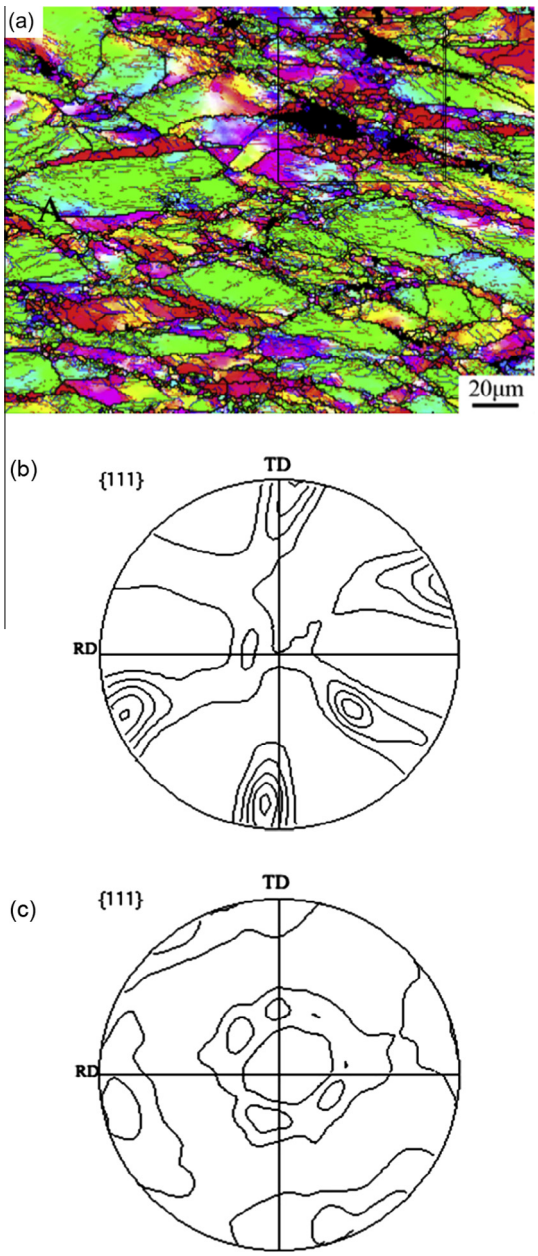

Fig. 7. The microstructure and the pole figures in different areas (a) the EBSD map of Fig. 2(a); (b) 111 pole figure from area around the large particle; (c) 111 pole figure from area remote from the particles.

3.5. Internal connections between mechanics and microstructures

The true stress–strain curves are uniform under the same strain rate except that the peak stresses are slightly different (in Fig. 8). When the strain is 0.34, stress exceeds peak value. At the same time, hardening behavior has already been finished, and reversion and resultant softening in the material begin, and the curve declines to some value. The nucleation of DRX grains and necklace formation made flow stresses abruptly drop in the following of work hardening region [26]. With the increase of strain ($\varepsilon = 0.68$), the curve declined steeply, and the DRX increased. Until the strain reached 1.2, the DRX rate softly cut down and the curve became leveled off. At the same time, dynamic softening reached equilibrium with dynamic hardening. It was considered that the fully DRX was performed in the tested steel. The corresponding microstructure is shown in Fig. 5(b).

In Fig. 8, LAGB indicates that misorientations angle is less than 15°, and TGB are Σ3 boundaries and Σ3-related variant twin grain boundaries, and *R* is the random HAGB. The numbers are their corresponding content percent in all GBs. At the beginning of the DRX process, the LAGB decreased, and the TGB increased and the stress reduced abruptly. And *R* fraction increased gently in the progress. Moreover, the increments of TGB and *R* were nearly equal to the amount of the decrement in the LAGB. This phenomenon can be interpreted by the mechanism of strain-induced boundary migration, in which LAGB migrated to random HAGBs, counteracted or

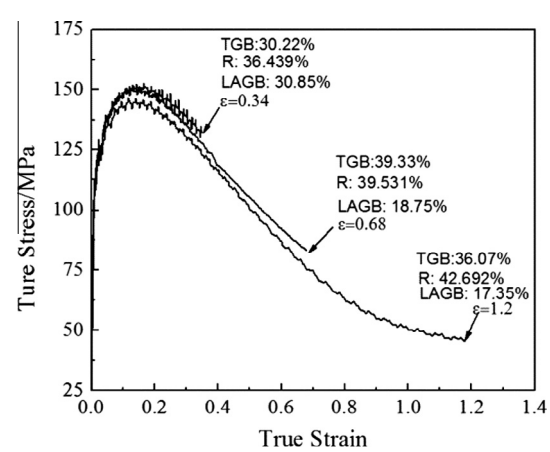

Fig. 8. True stress–strain curves and main GBCDs of specimens deformed at 1100 °C, 1 s^{-1} to different strain values.

swallowed by HAGBs during the process of DRX. Incidentally, the true stress reduced to 60 MPa when the strain changed from 0.34 to 0.68. However, at the end of the DRX, the changes of different types of misorientation angles fade away. When strain changed from 0.68 to 1.2, the difference of the LAGB was only 1.4%, while the fraction of TGB reduced amazingly. The trend of the low twin GB fractions observed here are consistent with other deformation methods in previous works, such as cold reductions between 5% and 60% [26]. At the same process, the true stress reduced about 30 MPa. Fig. 8 reveals that the stress decreased with the reduction of LAGBs percent. This result further confirms that mechanics and microstructure are intrinsically linked to each other.

4. Conclusions

Based on the investigation of hot deformation behavior and microstructural evolutions of a modified 310 austenitic stainless steel, some conclusions were drawn as follows:

(1) Coarsened precipitates at HAGBs strongly affected the occurrence of DRX. They not only promoted the nucleation but also prohibited the growth of the DRX grains.
(2) Large second phase particles broke up the planarity of the microstructure, and created a heterogeneous structure with equiangular grain near particles or locally randomized the deformed texture.
(3) In addition to the second particles, temperature and strain rate affected the process of DRX. Higher temperature and higher strain rate were favored for the occurrence of DRX. In misorientation distribution maps, there was a dominant effect of deformed temperatures on sub-grain boundaries. LAGBs decreased while HAGBs slowly increased with an increase of temperatures, consequently twin GBs and random HAGBs increased after deformed at higher temperatures.
(4) At high temperature and high strain rate, the true stress–strain curves exhibited tiny serrations effects due to the interaction of the DRX and precipitation. At the initial stage of DRX, the LAGB and twin GBs fraction changed greatly, and the stress dropped abruptly.

Acknowledgement

The authors thank the Foundation of Science and Technology on Reactor Fuel and Materials Laboratory for supporting to this research.

References

[1] Wang Man, Zhou Zhangjian, Sun Hongying, Hu Helong, Li Shaofu. Effects of plastic deformations on microstructure and mechanical properties of ODS-310 austenitic steel. Nucl Mater 2012;430:259–63.
[2] Dehghan-Manshadi A, Shokouhi A, Hodgson PD. Effect of isothermal dissolution and re-precipitation of austenite on the mechanical properties of duplex structures. Mater Sci Eng, A 2010;527:6765–70.
[3] Tan L, Sridharan K, Allen TR, Nanstad RK, McClintock DA. Microstructure tailoring for property improvements by grain boundary engineering. J Nucl Mater 2008;374:270–80.
[4] Belyakov A, Miura H, Sakai T. Dynamic recrystallization in ultrafine-grained 304 stainless steel. Scripta Mater 2000;43:21–6.
[5] Kim SI, Yoo YC. Dynamic recrystallization behavior of AISI 304 stainless steel. Mater Sci Eng, A 2001;311:108–13.
[6] Najafizadeh A, Jonas JJ, Stewart GR, Poliak EI. The strain dependence of post dynamic recrystallization in 304 H stainless steel. Metall Mater Trans 2006;37A:1899–906.
[7] Mataya MC, Nilsson ER, Brown EL, Krauss G. Hot working and recrystallization of As-Cast 316L. Metall Mater Trans 2003;34A:1683–703.
[8] Dehghan-Manshadi A, Barnett MR, Hodgson PD. Recrystallization in AISI 304 austenitic stainless steel during and after hot deformation. Mater Sci Eng, A 2008;485:664–72.
[9] Dehghan-Manshadi A, Beladi H, Barnett MR, Hodgson PD. Recrystallization in 304 austenitic stainless steel. Mater Sci Forum 2004;467–470:1163–8.
[10] Dehghan-Manshadi A, Barnett MR, Hodgson PD. Hot deformation and recrystallization of austenitic stainless steel: Part I. Dynamic recrystallization. Metall Mater Trans 2008;39A:1359–70.
[11] Momeni A, Shokuhfar A, Abbasi SM. Dynamic recrystallization of a Cr–Ni–Mo–Cu–Ti–V precipitation hardenable stainless steel. J Mater Sci Technol 2007;23:775–8.
[12] Mandal S, Sivaprasad PV, Dube RK, Raj B. Kinetics, Mechanism and modeling of microstructural evolution during dynamic recrystallization in a 15Cr–15Ni–2.2Mo–Ti modified austenitic stainless steel. Mater Sci Forum 2007;550:601–6.
[13] Mandal S, Sivaprasad PV, Dube RK. Kinetics, mechanism and modelling of microstructural evolution during thermo-mechanical processing of a 15Cr–15Ni–2.2Mo–Ti modified austenitic stainless steel. J Mater Sci 2007;42:2724–34.
[14] Ebrahimia GR, Keshmiria H, Momenib A, Mazinanic M. Dynamic recrystallization behavior of a superaustenitic stainless steel containing 16%Cr and 25%Ni. Mater Sci Eng, A 2011;528:7488–93.
[15] Rezaei Ashtiani HR, Parsa MH, Bisadi H. Effects of initial grain size on hot deformation behavior of commercial pure aluminum. Mater Des 2012;42:478–85.
[16] Vervynckta S, Verbekena K, Thibauxc bP, Houbaerta Y. Recrystallization–precipitation interaction during austenite hot deformation of a Nb microalloyed steel. Mater Sci Eng, A 2011;528:5519–28.
[17] Liu Guiwu, Han Ying, Shi Zhongqi, Sun Jiapeng, Zou Dening, Qiao Guanjun. Hot deformation and optimization of process parameters of an as-cast 6Mo superaustenitic stainless steel: a study with processing map. Mater Des 2014;53:662–72.
[18] Venugopal S, Mannan SL, Rodriguez P. Strategy for the design of thermo-mechanical processes for AISI type 304L stainless steel using dynamic materials model (DMM) stability criteria and model for the evolution of microstructure. J Mater Sci 2004;39:5557–60.
[19] El Wahabi M, Gavard L, Montheillet F, Cabrera JM, Prado JM. Effect of initial grain size on dynamic recrystallization in high purity austenitic stainless steels. Acta Mater 2005;53:4605–12.
[20] Momeni A, Dehghani K, Keshmiri H, Ebrahimi GR. Hot deformation behavior and microstructural evolution of a superaustenitic stainless steel. Mater Sci Eng, A 2010;527:1605–11.
[21] Yong QL. Second phases in structural steels. Beijing: Press of metallurgical industry; 2006. p. 15–100.
[22] Palumbo G, Aust KT, Lehockey EM, Erb U, Lin P. On a more restrictive geometric criterion for "special" CSL grain boundaries. Scripta Mater 1998;38:1685–90.
[23] Momeni A, Dehghani K. Microstructural evolution and flow analysis during hot working of a Fe–Ni–Cr superaustenitic stainless steel. Metall Mater Trans A 2011;42A:1925–32.
[24] Sekine M, Sakaguchi N, Endo M, Kinoshita H, Watanabe S, Kokawa H, et al. Grain boundary engineering of austenitic steel PNC316 for use in nuclear reactors. J Nucl Mater 2011;414:232–6.
[25] Ørsund R, Nes E. Effect of particles on recrystallization textures in aluminium-manganese alloys. Scripta Metall 1988;22:665–9.
[26] Yu YN. Principles of metallography. Beijng: Metallurgical Industry Press; 2003.